Tough-Hydrogel Reinforced Low-Tortuosity Conductive Networks for Stretchable and High-Performance Supercapacitors

Mutian Hua, Shuwang Wu, Yin Jin, Yusen Zhao, Bowen Yao, and Ximin He*

All-solid-state supercapacitors are seeing emerging applications in flexible and stretchable electronics. Supercapacitors with high capacitance, high power density, simple form factor, and good mechanical robustness are highly desired, which demands electrode materials with high surface area, high mass loading, good conductivity, larger thickness, low tortuosity, and high toughness. However, it has been challenging to simultaneously realize them in a single material. By compositing a superficial layer of tough hydrogel on conductive and low tortuous foams, a thick capacitor electrode with large capacitance (5.25 F cm^{-2}), high power density (41.28 mW cm^{-2}), and good mechanical robustness ($\varepsilon = 140\%$, $\Gamma = 1000$ J m^{-2}) is achieved. The tough hydrogel serves as both a load-bearing layer to maintain structural integrity during deformation and a permeable binder to allow interaction between the conductive electrode and electrolyte. It is shown that the tough hydrogel reinforcement is beneficial for both electrical and mechanical stability. With a simple design and facile fabrication, this strategy is generalizable for various conductive materials.

1. Introduction

Supercapacitors are an important class of energy storage device that are widely used for portable electronics, electric vehicles, and power plants.[1,2] Compared with metal-ion batteries, supercapacitors are advantageous in their high-power density, fast charging and discharging, and fire safety.[3] Traditional supercapacitors use liquid electrolytes, which make them bulky and difficult to seal. In recent years, supercapacitors can be readily fabricated using gel-electrolyte to obtain all-solid-state supercapacitors, adding light weight and simple form-factor to their advantages.[4–6]

Wearable and implantable electronics that are complaint and seamlessly function alongside a moving body have been actively developed for applications like artificial skin,[7] morphing sensors,[8] biomedical robots,[9,10] and human–machine interfacing.[11] For a prolonged period of untethered functioning

of these compliant electronics, energy storage devices like supercapacitors with high energy density, fast charging speed, and similar compliance are desired.[12,13] For this purpose, various polymeric materials have been used for improving the device flexibility and stretchability. For instance, hydrogels and aerogels are common polymeric scaffold materials for fabrication of supercapacitors.[5,14] Electrodes modified from hydrogel scaffolds generally retain the original material flexibility. With the intrinsic porous micro- and nanostructures of hydrogels, which yield high surface area and excellent permeability to ions, large capacitance and high rate capability are principally achievable.[15,16] The nonconductive elastic hydrogel scaffolds are often functionalized with conducting polymers like polypyrrole, polyaniline, poly(3,4-ethylenedioxythiophene):polystyrene sulfonate (PEDOT:PSS), and graphene for electrical conductivity,[17] using methods like infiltration by liquid-/vapor-phase and in situ polymerization.[18–27] However, the mass loading of conducting polymers by infiltration methods is relatively low (<10 mg cm^{-2}), as monomers are barricaded by the semicontinuous pores to diffuse into the hydrogel.[18–22] Therefore, only thin hydrogel electrodes are best compatible with this method to gain sufficient conductivity and electroactive material. The alternative in situ polymerization method can yield higher mass loadings;[23–27] however in particular cases, the solubility cap limits the maximum content of conducting polymers (e.g., pyrrole in water, PEDOT:PSS in water) in the aqueous solvent to stably coexist with the hydrogel monomers and the structure may vary significantly upon slight changes in the composition ratio.[23] "All-conducting-polymer" hydrogel electrodes have also been fabricated to show both flexibility and good conductivity.[28–32] However, these polymers may face embrittlement under stretching (strain <10%) and direct polymerization of the less soluble conducting polymers produces stacked spherical aggregates with poor electrical interconnection.[27] Successful methods involve using 2D conducting fillers[31] that are intrinsically robust and do not aggregate into spheres, synthesizing 1D conducting polymer fibers using special crosslinkers[30] and adding plasticizer agents.[33]

On the other hand, while thin electrodes are equally functional, thick electrodes offer the same capacitance with simpler device assembly and less usage of nonactive materials.

M. Hua, Dr. S. Wu, Y. Jin, Y. Zhao, Dr. B. Yao, Prof. X. He
Department of Materials Science and Engineering
University of California, Los Angeles
Los Angeles, CA 90095, USA
E-mail: ximinhe@ucla.edu

The ORCID identification number(s) for the author(s) of this article can be found under https://doi.org/10.1002/adma.202100983.

To increase the electrode thickness without reducing device efficiency and power density, low tortuosity electrodes, with aligned porous (anisotropic wood-like microstructure, low tortuosity in one direction) or even open porous structures (isotropic sponge-like microstructure, low tortuosity in all directions), are desired.[34–39] Strong macro-open-porous conducting foam materials have been used for fabricating supercapacitors with high thickness and low tortuosity. These macro-open-porous foams are fabricated by depositing conductive or electroactive materials on commercial metal foams or metallic textiles knitted by metal wires.[40–45] While excellent in mechanical stability, the low surface area will limit the mass loading, and thus the overall capacitance of the macro-open-porous electrodes. Alternatively, many micro-open-porous conductive hydrogels/aerogels showed both high surface area and low tortuosity. However, with microstructures of thin, brittle, and sparse interconnects, they are fragile due to the insufficient linkage between segments, and thus, are prone to mechanical damages during stretching. Therefore, creating robust micro-open-porous conducting foams would be advantageous in improving both the mechanical stability and power density of supercapacitors while maintaining high capacitance.

Here, we present a straightforward strategy for fabricating robust, low tortuosity electrodes with ultrahigh mass loading, by compositing a superficial layer of tough hydrogel as reinforcement binders to the originally fragile micro-open-porous conducting polymer electrodes, termed as tough-gel reinforced open-porous foam (TROF) in the following. We specifically selected poly(vinyl alcohol) (PVA) to construct the tough hydrogel layer due to its excellent mechanical properties,[46–48] ease of physical crosslinking,[49] and compositional simplicity. The ultratough hydrogel significantly reinforced the electrode even with a small amount of addition (0.1 mL cm^{-2}), which improved electrode flexibility, stretchability, and toughness while maintaining the open porous structure for fast diffusion. When assembled into an all-solid-state supercapacitor, the device demonstrated remarkably high capacitance (5.25 F cm^{-2}), power density (41.28 mW cm^{-2}), stretchability (140% strain), toughness (1000 J m^{-2}), and cyclic stability (95.8% capacitance retention after 3500 cycles), owing to the ultrahigh mass loading, open-porous structure, and tough hydrogel reinforcement. The presented strategy would greatly benefit the design and fabrication of high-performance supercapacitors for energy storage in flexible and wearable electronics.

2. Material Design and Fabrication

Figure 1A illustrates the design concept and fabrication procedure of the TROF electrode. Briefly, the initial open-porous conductive polymer foam was fabricated by the coaxial growth of conducting polymers on silver nanowires (Ag NWs, Figure S1, Supporting Information) in a mixture solution containing silver nanowires, pyrrole monomers, and oxidants. Similar reactions can be realized for various conducting polymers via a simple redox reaction.[38,39,50,51] The silver nanowires served as both a scaffold to guide the growth of polypyrrole (PPy) into an open-porous network (Figure 1B) and a highly conductive pathway to

improve the electrical transport in the thick electrode. The mass loading of active materials was tunable by adjusting the concentration of monomers (Figure S2, Supporting Information). Typically, the mass of PPy@Ag NWs foam is 32.2 mg cm^{-2} for samples made from precursor containing 10 vol% pyrrole. The open-porous conductive foam obtained after freeze drying was mechanically weak and difficult to process as supercapacitor electrodes (Figure 1B). The scanning electron microscopy (SEM) image showed the foam structure of sparely interconnected coaxial PPy@Ag NWs (Figure 1B). With an increase of pyrrole concentration from 2.5 to 25 vol% in the precursor mixture, the shell polypyrrole layer could exhibit morphology from smooth, to sphere decorated, and then to spherical agglomerate microstructures (Figure S2, Supporting Information). The final TROF was obtained by infiltrating a tough PVA hydrogel coating on the periphery of the open-porous conducting networks (Figure 1A). Benefiting from the low tortuous nature of the initial conducting polymer foam, the liquid PVA precursor (2–10 wt%) was quickly absorbed and spread inside the foams, which indicated that the penetration depth was much larger than the thickness of the fabricated foam (Figure S3, Movie S1, Supporting Information). After freezing and salting out in a 20 wt% lithium sulfate (Li$_2$SO$_4$) solution (Figure 1A), a tough and conducting electrode was obtained (Figure 1C). Li$_2$SO$_4$ was specifically chosen due to the high diffusivity of Li$^+$ ions and the good toughening effect of SO$_4^{2-}$ ions on PVA hydrogels.[52] We have also tested the conductivity of the electrode throughout the fabrication process to ensure that the TROF electrode maintains a good conductivity (Figure S4, Supporting Information). It was confirmed that the final TROF electrode has a conductivity comparable to the pristine foam.

Mechanistically, the infiltrated PVA solution spread inside the open porous foam following the contour of the conductive network due to surface tension. During freezing, the formation of ice crystals expelled the PVA polymers chains to the ice grain boundaries and induces the aggregation between PVA polymer chains.[49,53,54] Note that usually one-time freezing is insufficient to induce a strong aggregation between the PVA polymer chains, and only weak H-bond interaction was established during the freezing step.[55] Upon immersion into the high concentration lithium sulfate solution, in which the sulfate ions served as an efficient salting out agent by Hofmeister effect, the PVA polymer chains phase separated from the solution and formed strong crystalline domains by hydrogen bonding.[52,54,56–58] The densely aggregated PVA polymer chains lead to the formation of an ultrastrong and tough hydrogel (Figure S5, Supporting Information).[52,54] The toughening effect is strongly affected by the concentration of the infiltrated PVA solution. With the increase of PVA concentration from 2 to 10 wt%, the TROF electrode showed both increase in ultimate strain and stress by 200% and 1600%, respectively (Figure S6A, Supporting Information).

The ultratough PVA hydrogel reinforcement prepared by the freezing and salting out method allowed for significant reinforcement of the originally weak conducting polymer with only a thin coating of the tough hydrogel. The coating helped reduce diffusion barrier of ions to and from the encapsulated conductive network underneath and also maintain the desired open-porous microstructure (Figure 1C and Movie S2,
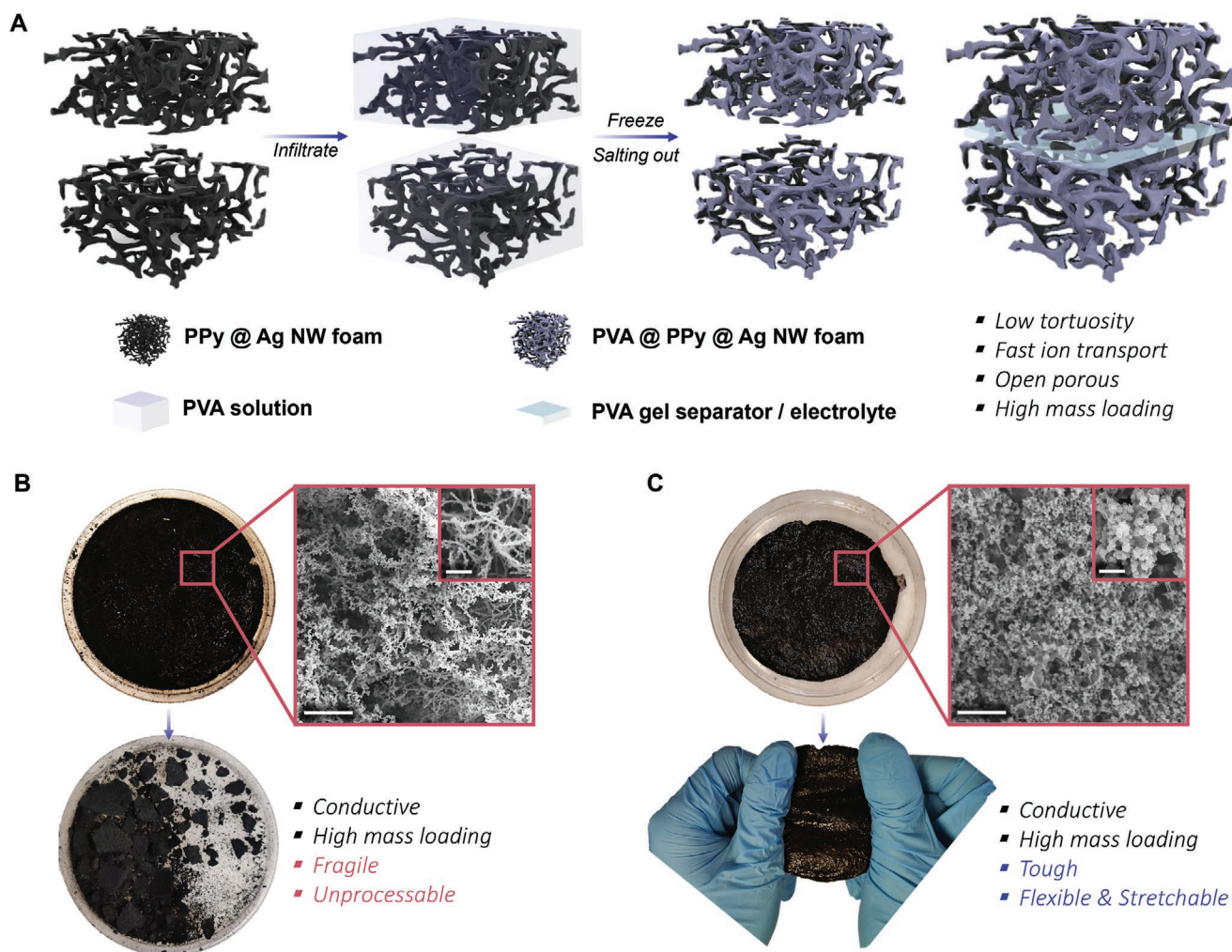
Figure 1. A) Schematic of the TROF electrode. B) PPy@Ag NWs foam without tough hydrogel reinforcement. The macroscopic image shows a black and open porous material that shatters easily under mechanical loading. The SEM image shows the microstructure of the foam. Scale bar: 50 µm; inset scale bar: 5 µm. C) PPy@Ag NWs foam with tough hydrogel reinforcement. The macroscopic image shows a black tough hydrogel reinforced PPy@Ag NWs foam composite that shows stretchability and mechanical robustness. The SEM image shows the microstructure of TROF. SEM scale bar: 50 µm; inset SEM scale bar: 5 µm; the diameter of the Petri dish is around 10 cm.

Supporting Information). Finally, an all-solid-state supercapacitor (**Figure 2**A) was fabricated by sandwiching a PVA hydrogel membrane between two pieces of 1.5 mm thick TROF electrode, the three layers were joint together by another cycle of freezing and salting out in a 20 wt% Li_2SO_4 + 5 wt% H_2SO_4 electrolyte solution.

3. Electrochemical Properties of the TROF Supercapacitor

We first evaluated the electrochemical performance of the TROF electrodes in a two-electrode system using the fabricated all-solid-state supercapacitor device. Variation in the pyrrole concentration from 2.5 to 25 vol% did not lead to significant change in the capacitance, as the ultimate surface area is mostly determined by the amount of Ag NWs (Figure S7, Supporting Information); however, higher concentration of pyrrole

yielded a lower internal resistance drop (Figure S6, Supporting Information) but higher hydrophobicity (Figure S3, Supporting Information). To ensure a balance between good conductivity, infiltration ability, and toughness, we used 10 vol% pyrrole precursors and 10 wt% PVA infiltration solution for the majority of the experiments. Figure 2B shows the typical CV curves of the TROF supercapacitor at various scan rates of 5–50 mV s^{-1}, the curves are all symmetric and has a near rectangular shapes at a scan rate below 10 mV s^{-1}, indicating a good capacitive behavior of the electrode. The Nyquist plots of the TROF supercapacitor showed a low equivalent series resistance of 7.3 Ω cm^2 and charge transfer resistance (R_{CT}) of 1.2 Ω cm^2, which benefited from the interconnected coaxial polypyrrole @ Ag NWs conductive network and the open-porous microstructure that facilitated the ion transportation (Figure 2C). The galvanostatic charge–discharge (GCD) curves measured with current density of 1–30 mA cm^{-2} within an operation window of 0–0.8 V all showed nearly triangular shapes, indicating the formation of
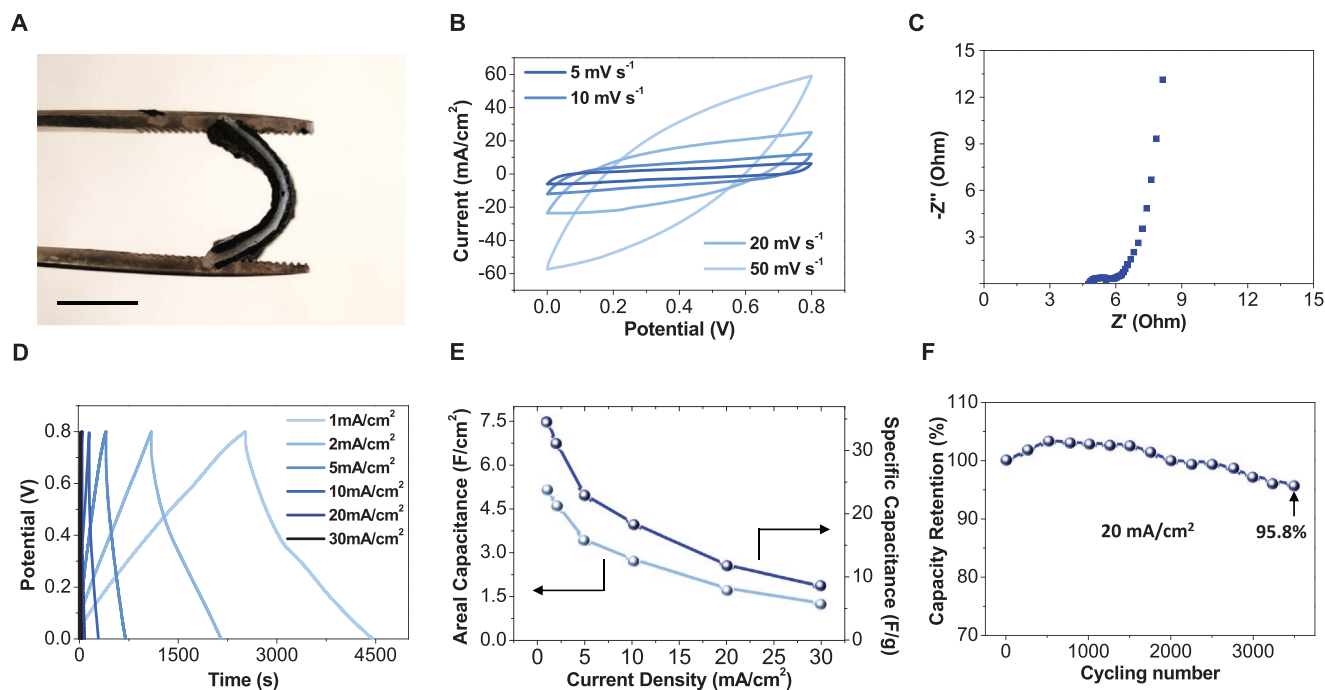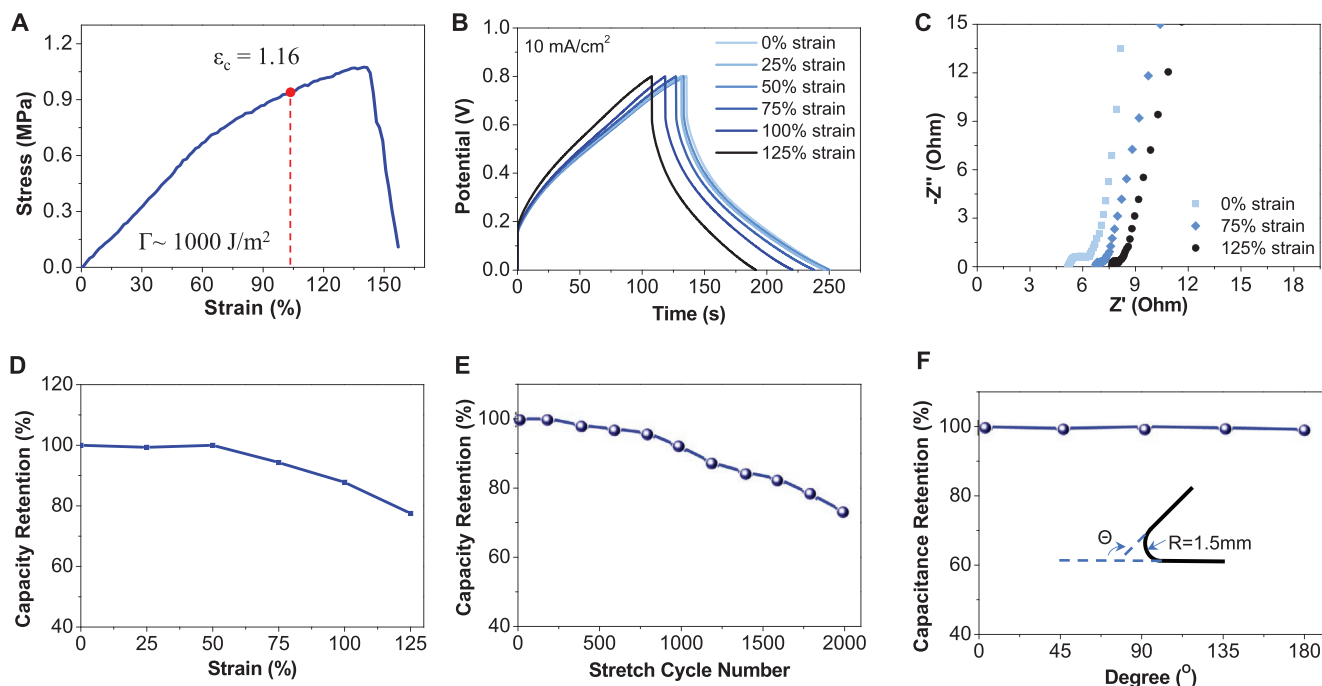
Figure 2. A) Image of the TROF supercapacitor fabricated by sandwiching two TROF electrodes and one PVA hydrogel separator. Scale bar: 5 mm. B) CV curves of TROF supercapacitor with scanning rate of 5–50 mV s^{-1}, device area 1 cm^2. C) Nyquist plot of TROF supercapacitor at frequencies from 0.1 MHz to 0.01 Hz. D) GCD curves of TROF supercapacitor at current densities of 1–30 mA cm^{-2}. E) Areal and specific capacitance of TROF supercapacitor at current densities of 1–20 mA cm^{-2}. F) Capacitance retention during 3500 GCD cycles.

efficient electrochemical double layer inside the TROF electrode and high Coulomb efficiency (Figure 2D). It should be noted that while a small amount of pseudo-capacitance (< 1%) may be contributed by the redox reaction of Ag NWs, it is negligible compared to that of the TROF electrode (Figure S8, Supporting Information). Remarkably, the TROF device exhibited an ultrahigh areal capacitance of 5.25 F cm^{-2} (34.96 F g^{-1}, normalized against the device's total weight) at 1 mA cm^{-2} charging and discharging rate (Figure 2E). Even at a high current density of 20 mA cm^{-2}, the areal capacitance was maintained at a high value of 1.8 F cm^{-2}, which indicated an excellent rate capability compared to most reported all-solid-state supercapacitors.[20,27,29,32,37] Surprisingly, with partial sacrifice of the mechanical robustness by infiltrating more dilute PVA solutions (2 wt% PVA), the areal capacitance of the device measured at the same high current density of 20 mA cm^{-2} increased for > 2 times to 3.9 F cm^{-2} (Figure S6B, Supporting Information). The capacitance values of the TROF are especially high, owing to the high mass loading of the electrodes (≈77 mg cm^{-2}). Such a high capacitance was maintained at 95.8% after 3500 GCD cycles even when operating under a high current density of 20 mA cm^{-2} (Figure 2F). The excellent cycling performance and stability were attributed to the open-porous structure that allowed fast ion-diffusion and the tough hydrogel reinforcement binder that maintained the structure integrity throughout the long-term GCD cycles. The capacitance reduction occurred at a much faster rate without the tough hydrogel reinforcement layer (Figure S9, Supporting Information), which indicated that the tough shell effectively helped maintain electrochemical stability of the electrode.

4. Mechanical Robustness of the TROF Device

Benefiting from the ultratough hydrogel reinforcement binder, the TROF electrode infiltrated with 10 wt% PVA and after salting out exhibited a high ultimate strength of ≈1 MPa and ultimate strain of ≈140%, which yields a toughness of 800 kJ m^{-3} and a fracture energy of ≈1000 J m^{-2} (**Figure 3**A). In contrast, the un-reinforced foam showed only ≈1 kPa strength and ≈15% strain, and the PVA infiltrate TROF electrode before salting out only slightly improved to ≈4 kPa strength and ≈40% strain (Figure S10, Supporting Information). Its resistance to fracture is comparable to cartilage[59] and many double-network tough hydrogels. We further evaluated the mechanical robustness of the supercapacitor device by recording the GCD curves under stretching (Figure 3B and Figure S11, Supporting Information). With a strain range of 0–125%, the internal resistance (IR) at 10 mA cm^{-2} of the stretched devices increased 1.5 times as tensile strain increased from 0% to 125% (Figure 3C). As a result, the GCD curves showed an increased IR drop with the increasing strain (Figure 3B). Normalized to weight, the specific capacitance of the stretched device showed no reduction at up to 50% strain, which indicated an intrinsic stretchability of the device (Figure 3D). With a strain higher than 50%, the device capacitance started to gradually reduce, ultimately to 76% of the original capacitance at 125% strain. However, the capacitance could be recovered upon releasing the strain, which indicated that the tough hydrogel layer protected the integrity of the microstructure during stretching (Figure S12, Supporting Information). The device showed good mechanical stability and maintained 73% of the original capacitance after

Figure 3. A) Stress–strain curve of TROF electrode. The red line marks the critical strain (ε_c) for onset of propagation of cracks in the material, the corresponding fracture energy is ≈ 1000 J m^{-2}. B) GCD curves of the TROF supercapacitor at a current density of 10 mA cm^{-2} when stretched to 0–125% strain. C) Nyquist plot of the TROF supercapacitor at frequencies from 0.1 MHz to 0.01 Hz when stretched to 0–125% strain. D) Capacitance retention of the TROF supercapacitor during stretching from 0% to 125% strain. E) Capacitance retention of the TROF supercapacitor during 2000 stretching cycles. F) Capacitance retention of the TROF supercapacitor when bending from 0° to 180°.

2000 mechanical cycles, each cycle was stretched to 125% strain (Figure 3E). A bending test was also carried out, where no significant capacitance change was observed for bending angle from 0° to 180° (Figure 3F).

5. Customization and Broad Application

In comparison to many other all-solid-state supercapacitors, a simple relationship that capacitance is positively correlated with mass loading becomes apparent (**Figure 4**A). The reported TROF supercapacitors demonstrated superior areal capacitance (5.25 F cm^{-2}) and energy density (0.46 mWh cm^{-2}), benefiting from the mostly conducting polymer structure, which ensured an ultrahigh mass loading (Figure 4A,B). Owing to the open porous structure created by coaxial growth of PPy on silver nanowires and maintained by the peripheral tough hydrogel binder, the TROF supercapacitors also showed high power density of 41.28 mW cm^{-2} in addition to a high energy density (Figure 4B).

The method for creating such a high-performance TROF electrode is simple and scalable (Figure 4C). The material size, shape, thickness, and performance could be tailored to application specifications by changing container geometry, monomer concentration, precursor volume, and hydrogel concentration. Due to the all-solid-state form factor, the TROF device is modular and could be serially connected for voltage increase (Figure S13, Supporting Information). Figure 4D shows a supercapacitor pack of two stacked TROF supercapacitors with a peak voltage of 1.6 V. The supercapacitor pack was connected

to a step-up voltage regulator to power a 5 V light-emitting diode (LED) light bulb (Movie S3 in the Supporting Information, the step-up voltage regulator has a minimum switch-on voltage of 1 V).

The presented strategy of reinforcing conductive polymer open-porous structures with tough hydrogel coating could also be expanded to many other material systems other than PPy. We further demonstrated the adaptation of the tough PVA/PPy@Ag NW system to PVA/PANi@Ag NW system and PVA/rGO system (Figure 4E and Figure S14, Supporting Information). Briefly, in fabricating PVA/PANi@Ag NW TROF electrodes, ammonia persulfate was used as the oxidant, and PVA was infiltrated following the same procedure as for the PVA/PPy@Ag NW system; while in fabricating PVA/rGO TROF electrodes, the open porous structure was directly obtained by freeze drying GO without Ag NWs, and reduced by infiltrating a PVA/hydroiodic acid (HI) solution. The PVA infiltrated foams were frozen and salted out in a 20 wt% LiSO$_4$ solution for toughening. In fabricating the PVA/rGO TROF electrode, silver nanowires were omitted due to the intrinsic superior high electrical conductivity of the rGO foam. Both PVA/PANi@Ag NW and PVA/rGO TROF electrodes showed 4.95 and 3.25 F cm^{-2} areal capacitance at 10 mA cm^{-2}, comparable to that of the PVA/polypyrrole@Ag NW TROF electrodes (Figure 4E).

6. Conclusion

In this study, we present a facile strategy to composite tough hydrogel and open-porous conducting polymer electrode
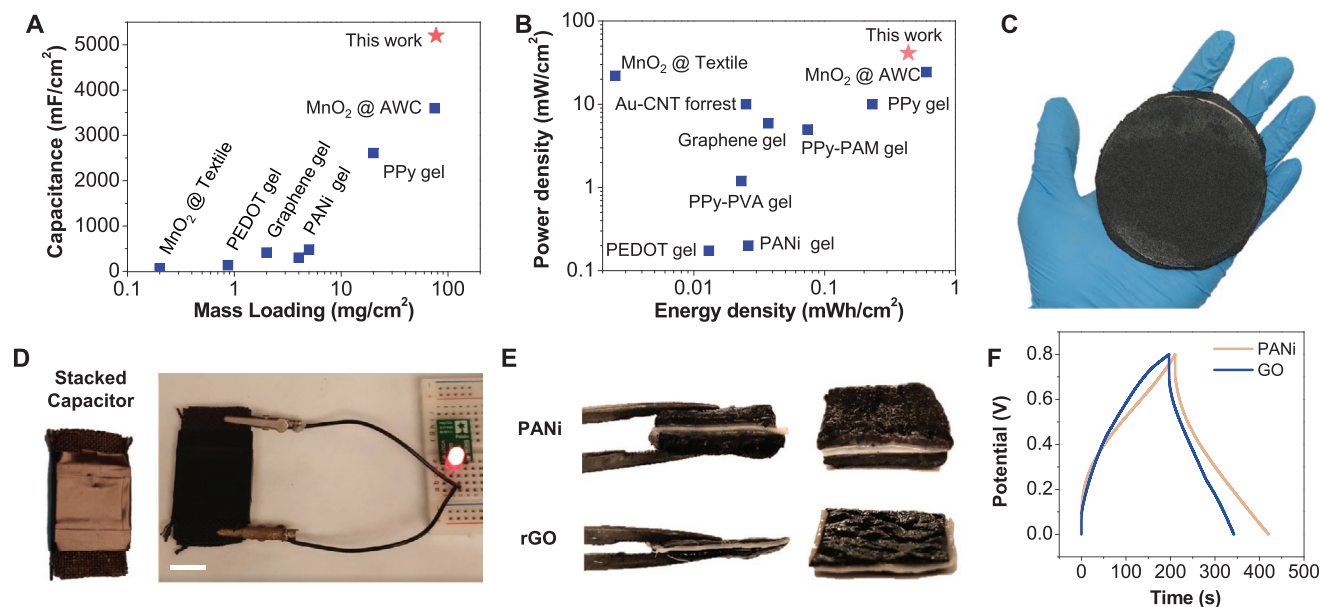
Figure 4. A) Areal capacitance versus mass loading of the TROF supercapacitor compared to other solid-state supercapacitors from the literature. B) Power density versus energy density loading of the TROF supercapacitor compared to other solid-state supercapacitors from the literature. C) Large-size TROF supercapacitor. The diameter of the device is 10 cm. D) Stacked TROF supercapacitor with a peak output voltage of 1.6 V powers a 5 V LED using a step-up voltage regulator. Scale bar: 1 cm. E) TROF supercapacitor made from PANi@Ag NWs foam and rGO foam. F) GCD cycles of TROF supercapacitors made from open-porous PANi@Ag NWs foam and rGO foam.

through infiltration of tough hydrogel precursor and subsequent gelation by freezing-assisted salting out. The resulting composite electrodes presented an open-porous microstructure covered by a superficial tough hydrogel layer, which harnessed simultaneous mechanical robustness, high surface area, and low tortuosity. With the combined properties, the assembled all-solid-state supercapacitor based on the TROF electrode showed simultaneous high capacitance (5.25 F cm^{-2}), energy density (0.46 mWh cm^{-2}), power density (41.28 mW cm^{-2}), stretchability (140%), and fracture toughness (1000 J cm^{-2}). Benefitting from the tough hydrogel reinforcement, the supercapacitor showed good electrical stability (95.8% after 3500 GCD cycles) and mechanical stability (73% after 2000 mechanical cycles) with a moderate reduction in performance. With the presented facile method for coating tough hydrogel reinforcement layer and various conducting foam materials available, the presented strategy could be expanded to other electrode systems for bringing improvements in stretchability and toughness of electrode. We foresee that many fine structures used in energy storage, sensing, and robotic fields could be strengthened using the presented strategy and we are convinced that compositing tough hydrogel and these fine structures opens up new opportunities for the application of structural hydrogel in the fields of energy storage, sensing, soft robotics, and stretchable electronic devices.

7. Experimental Section

Materials: Silver nitrate (AgNO$_3$, Fisher Scientific, 99%), ethylene glycol (Fisher Scientific), poly(vinylpyrrolidone) (PVP, M.W. 360 000, Fisher Scientific), pyrrole (reagent grade, 98%, Sigma Aldrich), aniline

(98%, Sigma Aldrich), graphene oxide (4 mg mL^{-1}, Sigma Aldrich), HI (55%, Sigma Aldrich), ammonia persulfate (APS, Sigma Aldrich), PVA (M.W. = 89 000–98 000, 99% hydrolyzed, Sigma Aldrich), and iron(III) chloride (FeCl$_3$, Sigma Aldrich) were all used as received.

Fabrication of the Silver Nanowires: A facile polyol synthesis procedure of Ag NWs was used.[60] Briefly, 1 g of PVP was added to 100 mL of ethylene glycol and completely dissolved by stirring under room temperature. Subsequently, 1 g of AgNO$_3$ was added to the solution and completely dissolved. Afterward, 10 mL of FeCl$_3$ (1×10^{-3} M in ethylene glycol) solution was added to the mixture and stirred for 1 min. The mixture was immediately transferred to an oil bath preheated to 110 °C and left still to grow Ag NWs for 12 h. The obtained Ag NWs were then centrifuged and washed by ethanol for three times and finally dispersed in ethanol for later use (Figure S1, Supporting Information). The final Ag NWs dispersion had a concentration of ≈3 mg mL^{-1} measured by weighing the air-dried residue of the solution.

Fabrication of the PPy@Ag NWs Foam: The PPy@Ag NWs foam was fabricated by mixing two parts of a precursor together. Precursor part A: 2x vol% pyrrole dissolved in 7.5 mL of Ag NWs solution (solvent: ethanol). Precursor part B: 1.17x wt% FeCl$_3$ dissolved in 7.5 mL water (Fe^{3+} and pyrrole molar ratio was adjusted to be 1:4, x = 2.5, 5, 10, 25). The two parts of the precursor were cooled in a −20 °C freezer for 10 min before mixing the precursor parts A and B together. After mixing the precursor parts A and B together, the final mixture containing x vol% pyrrole and y wt% FeCl$_3$ was vortexed for 10 s and poured into a Petri dish and stored in a 4 °C fridge for 12 h. Finally, the resulting gel-like product was washed with ethanol to remove excess pyrrole monomer and immersed in deionized (DI) water for 24 h to remove other nonreacted chemicals. The washed sample was then freeze-dried using a Labconco Freezone freeze-dryer to obtain the micro-open-porous PPy@Ag NWs foam.

Fabrication of the PANi@Ag NWs and rGO Foam: For synthesizing micro-open-porous PANi@Ag NWs foam, the fabrication procedure mostly followed the case of PPy @Ag NWs foam described in the previous section with a few modifications. Precursor A was modified to have 2x vol% aniline dissolved in 7.5 mL of Ag NWs solution (solvent: water). Precursor B was modified to have 2y wt% APS dissolved in 7.5 mL water (APS and aniline ratio was also 1:4). For synthesizing

micro-open-porous rGO foam, aqueous graphene oxide solution (10 mg mL^{-1}) was directly freeze-dried and then reduced using a 2 wt% HI solution.

Fabrication of the TROF: 2–10 wt% PVA solution was prepared by dissolving PVA in DI water under heating and stirring to achieve a homogenous solution. The PVA solution was added dropwise into the micro-open-porous PPy@Ag NWs foam using a pipet. The volume of the added PVA solution was fixed at 0.1 mL cm^{-2}. The PVA infiltrated foam was left still for homogenization for 10 min and then put in a −20 °C freezer for 1 h until completely frozen. The frozen sample was then cast into 20 wt% Li$_2$SO$_4$ solution for 30 min for salting out toughening to obtain the TROF electrode.

Assembly of the Supercapacitor: The surface of the TROF in contact with the current collector was sanded slightly to reduce the resistance between the electrode and carbon cloth current collector. Then, a gel separator film was fabricated by freezing 5 wt% PVA solution followed by subsequent sating out in a 20 wt% Li$_2$SO$_4$ solution for 30 min for physically crosslinking the PVA. The gel separator film was sandwiched between two TROF electrodes and pressed together. The assembled supercapacitor was then frozen and salted out for another cycle in 20 wt% Li$_2$SO$_4$ + 5 wt% H$_2$SO$_4$ electrolyte solution to adhere the three layers together.

Electrochemical Characterization: The electrochemical properties were characterized by a CHI660E electrochemical workstation using a two-electrode setup. Two pieces of carbon cloth were used as current collectors in contact with the TROF electrodes.

Mechanical Characterization: The mechanical property characterization and stretchable supercapacitor study was carried out using a Univert mechanical tester with 450 mN loading cell.

Materials Characterization: The SEM images of samples were taken using a Supra 40VP scanning electron microscope.

Supporting Information

Supporting Information is available from the Wiley Online Library or from the author.

Acknowledgements

Conflict of Interest

The authors declare no conflict of interest.

Author Contributions

M.H. and S.W. contributed equally to this work. M.H., S.W., and X.H. conceived the concept. X.H. supervised the project. M.H. and K.J. conducted the experiments. S.W, Y.Z., and B.Y helped with the result analysis. M.H. wrote the initial draft. All authors contributed to the discussion of the manuscript.

Data Availability Statement

The data that support the findings of this study are available from the corresponding author upon reasonable request.

[1] F. Wang, X. Wu, X. Yuan, Z. Liu, Y. Zhang, L. Fu, Y. Zhu, Q. Zhou, Y. Wu, W. Huang, *Chem. Soc. Rev.* **2017**, *46*, 6816.
[2] J. R. Miller, P. Simon, *Science* **2008**, *321*, 651.
[3] P. Simon, Y. Gogotsi, B. Dunn, *Science* **2014**, *343*, 1210.
[4] X. Lu, M. Yu, G. Wang, Y. Tong, Y. Li, *Energy Environ. Sci.* **2014**, *7*, 2160.
[5] D. P. Dubal, N. R. Chodankar, D. H. Kim, P. Gomez-Romero, *Chem. Soc. Rev.* **2018**, *47*, 2065.
[6] T. Lv, M. Liu, D. Zhu, L. Gan, T. Chen, *Adv. Mater.* **2018**, *30*, 1705489.
[7] J. C. Yang, J. Mun, S. Y. Kwon, S. Park, Z. Bao, S. Park, *Adv. Mater.* **2019**, *31*, 1904765.
[8] Y. Liu, J. Li, S. Song, J. Kang, Y. Tsao, S. Chen, V. Mottini, K. McConnell, W. Xu, Y. Q. Zheng, J. B. H. Tok, P. M. George, Z. Bao, *Nat. Biotechnol.* **2020**, *38*, 1031.
[9] Y. Kim, G. A. Parada, S. Liu, X. Zhao, *Sci. Rob.* **2019**, *4*, eaax7329.
[10] Y. Zhao, C.-Y. Lo, L. Ruan, C.-H. Pi, C. Kim, Y. Alsaid, I. Frenkel, R. Rico, T.-C. Tsao, X. He, *Sci. Rob.* **2021**, *6*, eabd5483.
[11] Y. Kim, A. Chortos, W. Xu, Y. Liu, J. Y. Oh, D. Son, J. Kang, A. M. Foudeh, C. Zhu, Y. Lee, S. Niu, J. Liu, R. Pfattner, Z. Bao, T. W. Lee, *Science* **2018**, *360*, 998.
[12] D. G. Mackanic, M. Kao, Z. Bao, *Adv. Energy Mater.* **2020**, *10*, 2001424.
[13] D. G. Mackanic, T. H. Chang, Z. Huang, Y. Cui, Z. Bao, *Chem. Soc. Rev.* **2020**, *49*, 4466.
[14] L. Li, Z. Lou, D. Chen, K. Jiang, W. Han, G. Shen, *Small* **2018**, *14*, e1702829.
[15] S. Ghosh, O. Inganäs, *Adv. Mater.* **1999**, *11*, 1214.
[16] M. Salanne, B. Rotenberg, K. Naoi, K. Kaneko, P. L. Taberna, C. P. Grey, B. Dunn, P. Simon, *Nat. Energy* **2016**, *1*, 16070.
[17] F. Zhao, J. Bae, X. Zhou, Y. Guo, G. Yu, *Adv. Mater.* **2018**, *30*, 1801796.
[18] Y. Guo, K. Zheng, P. Wan, *Small* **2018**, *14*, e1704497.
[19] K. Wang, X. Zhang, C. Li, X. Sun, Q. Meng, Y. Ma, Z. Wei, *Adv. Mater.* **2015**, *27*, 7451.
[20] L. Zang, Q. Liu, J. Qiu, C. Yang, C. Wei, C. Liu, L. Lao, *ACS Appl. Mater. Interfaces* **2017**, *9*, 33941.
[21] Y. Zhao, Y. Alsaid, B. Yao, Y. Zhang, B. Zhang, N. Bhuskute, S. Wu, X. He, *Adv. Funct. Mater.* **2020**, *30*, 1909133.
[22] G. P. Hao, F. Hippauf, M. Oschatz, F. M. Wisser, A. Leifert, W. Nickel, N. Mohamed-Noriega, Z. Zheng, S. Kaskel, *ACS Nano* **2014**, *8*, 7138.
[23] P. Li, Z. Jin, L. Peng, F. Zhao, D. Xiao, Y. Jin, G. Yu, *Adv. Mater.* **2018**, *30*, 1800124.
[24] W. Li, F. Gao, X. Wang, N. Zhang, M. Ma, *Angew. Chem., Int. Ed.* **2016**, *55*, 9196.
[25] Q. Chen, H. Lu, F. Chen, L. Chen, N. Zhang, M. Ma, *ACS Appl. Energy Mater.* **2018**, *1*, 4261.
[26] B. S. Yin, S. W. Zhang, Q. Q. Ren, C. Liu, K. Ke, Z. B. Wang, *J. Mater. Chem. A* **2017**, *5*, 24942.
[27] Y. Zhao, B. Zhang, B. Yao, Y. Qiu, Z. Peng, Y. Zhang, Y. Alsaid, I. Frenkel, K. Youssef, Q. Pei, X. He, *Matter* **2020**, *3*, 1196.
[28] E. P. Gilshteyn, D. Amanbayev, A. S. Anisimov, T. Kallio, A. G. Nasibulin, *Sci. Rep.* **2017**, *7*, 17449.

**ADVANCED
SCIENCE NEWS**

www.advancedsciencenews.com

**ADVANCED
MATERIALS**

www.advmat.de

[29] C. Chen, Y. Zhang, Y. Li, J. Dai, J. Song, Y. Yao, Y. Gong, I. Kierzewski, J. Xie, L. Hu, *Energy Environ. Sci.* **2017**, *10*, 538.

[30] Y. Wang, Y. Shi, L. Pan, Y. Ding, Y. Zhao, Y. Li, Y. Shi, G. Yu, *Nano Lett.* **2015**, *15*, 7736.

[31] Y. Xu, Z. Lin, X. Huang, Y. Wang, Y. Huang, X. Duan, *Adv. Mater.* **2013**, *25*, 5779.

[32] Y. Shi, L. Pan, B. Liu, Y. Wang, Y. Cui, Z. Bao, G. Yu, *J. Mater. Chem. A* **2014**, *2*, 6086.

[33] Y. Wang, C. Zhu, R. Pfattner, H. Yan, L. Jin, S. Chen, F. Molina-Lopez, F. Lissel, J. Liu, N. I. Rabiah, Z. Chen, J. W. Chung, C. Linder, M. F. Toney, B. Murmann, Z. Bao, *Sci. Adv.* **2017**, *3*, e1602076.

[34] Y. Wang, X. Lin, T. Liu, H. Chen, S. Chen, Z. Jiang, J. Liu, J. Huang, M. Liu, *Adv. Funct. Mater.* **2018**, *28*, 1806207.

[35] C. Chen, Y. Zhang, Y. Li, Y. Kuang, J. Song, W. Luo, Y. Wang, Y. Yao, G. Pastel, J. Xie, L. Hu, *Adv. Energy Mater.* **2017**, *7*, 1700595.

[36] X. L. Wu, T. Wen, H. L. Guo, S. Yang, X. Wang, A. W. Xu, *ACS Nano* **2013**, *7*, 3589.

[37] W. Chen, R. B. Rakhi, L. Hu, X. Xie, Y. Cui, H. N. Alshareef, *Nano Lett.* **2011**, *11*, 5165.

[38] W. He, G. Li, S. Zhang, Y. Wei, J. Wang, Q. Li, X. Zhang, *ACS Nano* **2015**, *9*, 4244.

[39] J. Zhou, L. Yu, W. Liu, X. Zhang, W. Mu, X. Du, Z. Zhang, Y. Deng, *Sci. Rep.* **2015**, *5*, 17858.

[40] H. Park, J. W. Kim, S. Y. Hong, G. Lee, D. S. Kim, J. hyun Oh, S. W. Jin, Y. R. Jeong, S. Y. Oh, J. Y. Yun, J. S. Ha, *Adv. Funct. Mater.* **2018**, *28*, 1707013.

[41] T. Purkait, G. Singh, D. Kumar, M. Singh, R. S. Dey, *Sci. Rep.* **2018**, *8*, 640.

[42] G. Shao, R. Yu, X. Zhang, X. Chen, F. He, X. Zhao, N. Chen, M. Ye, X. Y. Liu, *Adv. Funct. Mater.* **2020**, *30*, 2003153.

[43] W. Li, M. C. Tekell, C. Liu, J. A. Hethcock, D. Fan, *Adv. Funct. Mater.* **2018**, *28*, 1800601.

[44] Z. Ren, Y. Li, J. Yu, *iScience* **2018**, *9*, 138.

[45] X. Zhang, J. Zhao, T. Xia, Q. Li, C. Ao, Q. Wang, W. Zhang, C. Lu, Y. Deng, *Energy Storage Mater.* **2020**, *31*, 135.

[46] S. Lin, J. Liu, X. Liu, X. Zhao, *Proc. Natl. Acad. Sci. USA* **2019**, *116*, 10244.

[47] S. Lin, X. Liu, J. Liu, H. Yuk, H.-C. Loh, G. A. Parada, C. Settens, J. Song, A. Masic, G. H. McKinley, X. Zhao, *Sci. Adv.* **2019**, *5*, eaau8528.

[48] R. Bai, J. Yang, X. P. Morelle, Z. Suo, *Macromol. Rapid Commun.* **2019**, *40*, 1800883.

[49] H. Zhang, *Ice Templating and Freeze-Drying for Porous Materials and Their Applications*, Wiley-VCH, Weinheim, Germany **2018**.

[50] R. Liu, B. L. Sang, *J. Am. Chem. Soc.* **2008**, *130*, 2942.

[51] M. Gao, S. Huang, L. Dai, G. Wallace, R. Gao, Z. Wang, *Angew. Chem., Int. Ed.* **2000**, *39*, 3664.

[52] S. Wu, M. Hua, Y. Alsaid, Y. Du, Y. Ma, Y. Zhao, C.-Y. Lo, C. Wang, D. Wu, B. Yao, J. Strzalka, H. Zhou, X. Zhu, X. He, *Adv. Mater.* **2021**, *33*, 2007829.

[53] H. Zhang, I. Hussain, M. Brust, M. F. Butler, S. P. Rannard, A. I. Cooper, *Nat. Mater.* **2005**, *4*, 787.

[54] M. Hua, S. Wu, Y. Ma, Y. Zhao, Z. Chen, I. Frenkel, J. Strzalka, H. Zhou, X. Zhu, X. He, *Nature* **2021**, *590*, 594.

[55] S. Gupta, S. Goswami, A. Sinha, *Biomed. Mater.* **2012**, *7*, 015006.

[56] P. Van De Witte, P. J. Dijkstra, J. W. A. Van Den Berg, J. Feijen, *J. Membr. Sci.* **1996**, *117*, 1.

[57] M. Iwaseya, M. Watanabe, K. Yamaura, L. X. Dai, H. Noguchi, *J. Mater. Sci.* **2005**, *40*, 5695.

[58] S. Paṭachia, C. Florea, C. Friedrich, Y. Thomann, *eXPRESS Polym. Lett.* **2009**, *3*, 320.

[59] N. K. Simha, C. S. Carlson, J. L. Lewis, *J. Mater. Sci.: Mater. Med.* **2004**, *15*, 631.

[60] J. Jiu, T. Araki, J. Wang, M. Nogi, T. Sugahara, S. Nagao, H. Koga, K. Suganuma, E. Nakazawa, M. Hara, H. Uchida, K. Shinozaki, *J. Mater. Chem. A* **2014**, *2*, 6326.